Region-Wide Glacier Mass Budgets for the Tanggula Mountains between ~1969 and ~2015 Derived from Remote Sensing Data

Authors: Chen, An'an, Wang, Ninglian, Li, Zhen, Wu, Yuwei, Zhang, Wei, et al.

Source: Arctic, Antarctic, and Alpine Research, 49(4) : 551-568

Published By: Institute of Arctic and Alpine Research (INSTAAR), University of Colorado

URL: https://doi.org/10.1657/AAAR0016-065

Arctic, Antarctic, and Alpine Research, Vol. 49, No. 4, 2017, pp. 551–568
DOI: http://dx.doi.org/10.1657/AAAR0016-065

Region-wide glacier mass budgets for the Tanggula Mountains between ~1969 and ~2015 derived from remote sensing data

An'an Chen[1,4], Ninglian Wang[2,3,*], Zhen Li[1], Yuwei Wu[2,3], Wei Zhang[1], and Zhongming Guo[2,3]

[1]State Key Laboratory of Cryospheric Science, Northwest Institute of Eco-Environment and Resources, Chinese Academy of Sciences, Lanzhou, Gansu 730000, China
[2]Shaanxi Key Laboratory of Earth Surface System and Environmental Carrying Capacity, Xi'an, Shaanxi Province 710127, China
[3]Institute of Earth Surface System and Hazards, College of Urban and Environmental Sciences, Northwest University, Xi'an, Shaanxi Province 710127, China
[4]University of Chinese Academy of Sciences, Beijing 100049, China
[*]Corresponding author's email: nlwang@nwu.edu.cn

A B S T R A C T

Temporal changes in the properties of glaciers located on the central Tibetan Plateau are a sensitive indicator of climate change and the water supply. To estimate the region-wide glacier budgets for three study sites covering the region extending from West-Geladandong to Bugyai Kangri, we compared 1968/1969 topographic maps, the 2000 SRTM DEM, and recent ASTER DEMs for glacier mass budget calculations. Between ~1969 and ~2015, the specific mass budget was –0.31 ± 0.05 m w.e. a^{-1} for the entire Tanggula Mountains, which is lower than the global average. This ongoing mass loss is mainly caused by increasing summer temperatures since the 1960s. Heterogeneous glacier behavior can be explained by a combination of factors, including meteorological conditions, proglacial lakes, and surge-type glaciers.

Introduction

High Mountain Asia (HMA) has the greatest density of glaciers outside of the polar regions, and the glacier meltwater produced in this region has a significant impact on global sea level rise and regional water resources (Immerzeel et al., 2010; Kaser et al., 2010; Yao et al., 2012). During 2003–2009, the amount of glacier mass lost from HMA was equivalent to a global sea level rise of ~0.13 ± 0.04 mm a^{-1} (Matsuo and Heki, 2010), and 1.7 ± 1.9 Gt a^{-1} of the glacier meltwater drained into endorheic basins on the Tibetan Plateau (Neckel et al., 2014). The rapid glacier retreat has enhanced runoff from the Tibetan Plateau in northwest China by more than 5.5% since the last decade of the 20th century (Yao et al., 2007), and glacier meltwater from the Himalayas has contributed ~3.5% and ~2.0% of the annual average river discharge of the Indus and Ganges basins, respectively (Kääb et al., 2012).

Mass balance is the most useful and direct metric of glacier change (Bolch et al., 2011). Glaciological and geodetic methods provide two different means of calculating mass balance (Zemp et al., 2015). The earliest glaciological observations of mass balance started in Europe and Scandinavia in the 1940s, followed by HMA in the 1950s (Zemp et al., 2009). The geodetic method involves the comparison of multi-temporal elevation data sets, and its history can be traced back to the early 20th century (Zemp et al., 2015). The glaciological method provides reliable and high-temporal-resolution glacier mass balance estimates; however, the number of glaciological monitoring sites is small because glaciers are located in remote alpine and high-latitude regions. For example, the mass balance has been measured on only 26 out

of the 85,700 glaciers of HMA, and only one glacier on the inner Tibetan Plateau, the Xiao Dongkemadi glacier (XDG), has more than 20 years of mass balance records (Pu et al., 2008; Yao et al., 2010a; Wang et al., 2013; Yu et al., 2013; Zemp et al., 2013; Arendt et al., 2015; Tshering and Fujita., 2016). With the development of geodetic technology and the increased availability of elevation data, the geodetic method provides thickness and volume change information for large samples of glaciers that span entire mountain ranges, which is important for quantifying the contributions from glacier meltwater to hydrological processes. Mass budget estimates on the Tibetan Plateau have been obtained using geodetic methods since the mid-20th century (Bolch et al., 2008; Wang et al., 2013; Neckel et al., 2014; Yi and Sun, 2014). Existing studies have mainly focused on the Himalayas and the Karakoram, western Kunlun, and Tien Shan mountain ranges (Gardelle et al., 2013; Ke et al., 2015a; Pieczonka and Bolch, 2015). However, there are currently no region-wide glacier mass budgets for larger regions or entire mountain ranges in the Tanggula Mountains.

The Tanggula Mountains represent an important climatic divide on the Tibetan Plateau. The delivery of moisture to their southern slopes is influenced mainly by the Indian monsoon, whereas it is controlled primarily by continental air masses on the northern slopes (Tian et al., 2001; Li et al., 2015). The Dongkemadi region is located within the Tanggula Mountains. The China–Japan Joint Expedition launched the first systematic investigation of this region in 1989, and intensive glaciological studies have continued since then (Fujita and Ageta, 2000; Gao et al., 2012; Huang et al., 2013; Wu et al., 2015; Li et al., 2016; Shi et al., 2016). Although the mass budgets of glaciers in the Dongkemadi region have been calculated from 1969 to 2009 using multiple geodetic methods (Shangguan et al., 2008; Li et al., 2012; Ke et al., 2015b), glacier mass budgets have not been presented for the entire Tanggula Mountains.

This study has three aims. The main objective is to assess the region-wide glacier mass budgets for the entire Tanggula Mountains from ~1969 to ~2015. The second objective aims to verify the mass budgets calculated using glaciological and geodetic methods. The third objective is to investigate spatial patterns of glacier mass change and to discuss the potential reasons for these changes.

Study Area

The Tanggula Mountains are located within the central Tibetan Plateau, extending from the Chibzhang Co in the northwest to the Bugyai Kangri in the southeast. They serve as a geographical boundary between the Yangtze and Nujiang river basins (Yao et al., 2010b). The highest peak of the Tanggula Mountains is located in the Geladandong range, with an elevation of 6621 m above sea level (m a.s.l.). According to the Second Glacier Inventory Dataset of China, the total glacier-covered area of the Tanggula Mountains was 1843.9 km^2 in 2007 (Liu et al., 2015). In this study, mass budgets are determined for three study sites spreading across the Tanggula Mountains to capture the glaciological variability of the entire mountain range. The locations of each study site are displayed in Figure 1, together with the extent of the corresponding subregions used to extrapolate the mass budgets for the entire Tanggula Mountains. The eastern site (Bugyai Kangri) is mainly influenced by the Indian monsoon (Gardelle et al., 2013), whereas the Indian monsoon and continental air masses are dominating the northwestern sites (Dongkemadi and West-Geladandong) (Tian et al., 2001).

Systematic glaciological and meteorological observations have been performed since 1989 in the Dongkemadi river basin. The mean annual temperature is approximately –6.0 °C. In 2009, the annual precipitation was 622 mm, of which >90% fell during the summer months of June–August (He et al., 2009). The highest monthly average temperatures (>0 °C) occurred during June–September (Li et al., 2015). Glaciological mass balance has been measured at the XDG since 1989.

Data and Methods

Topographic maps, Landsat TM/OLI, Terra ASTER images, and SRTM1 data were used to obtain information about glacier boundaries and surface elevations in different periods. Detailed information on the remote sensing data used is listed in Table 1.

DEM Generation and Evaluation

Topographic Maps

Three 1:100,000-scale topographic maps were produced in 1973 and 1974, respectively. Aerial photographs were acquired in 1969 for Dongkemadi and West-Geladandong and in 1968 for Bugyai Kangri. The equidistant elevation of the 1:100,000-scale topographic map is 20 m, and the nominal vertical accuracies of these topographic maps were within 5 m for areas with slopes <6° and 8 m for areas with slopes between 6° and 25°, according to the China National Standard for Photogrammetry (State Bureau of Sur-

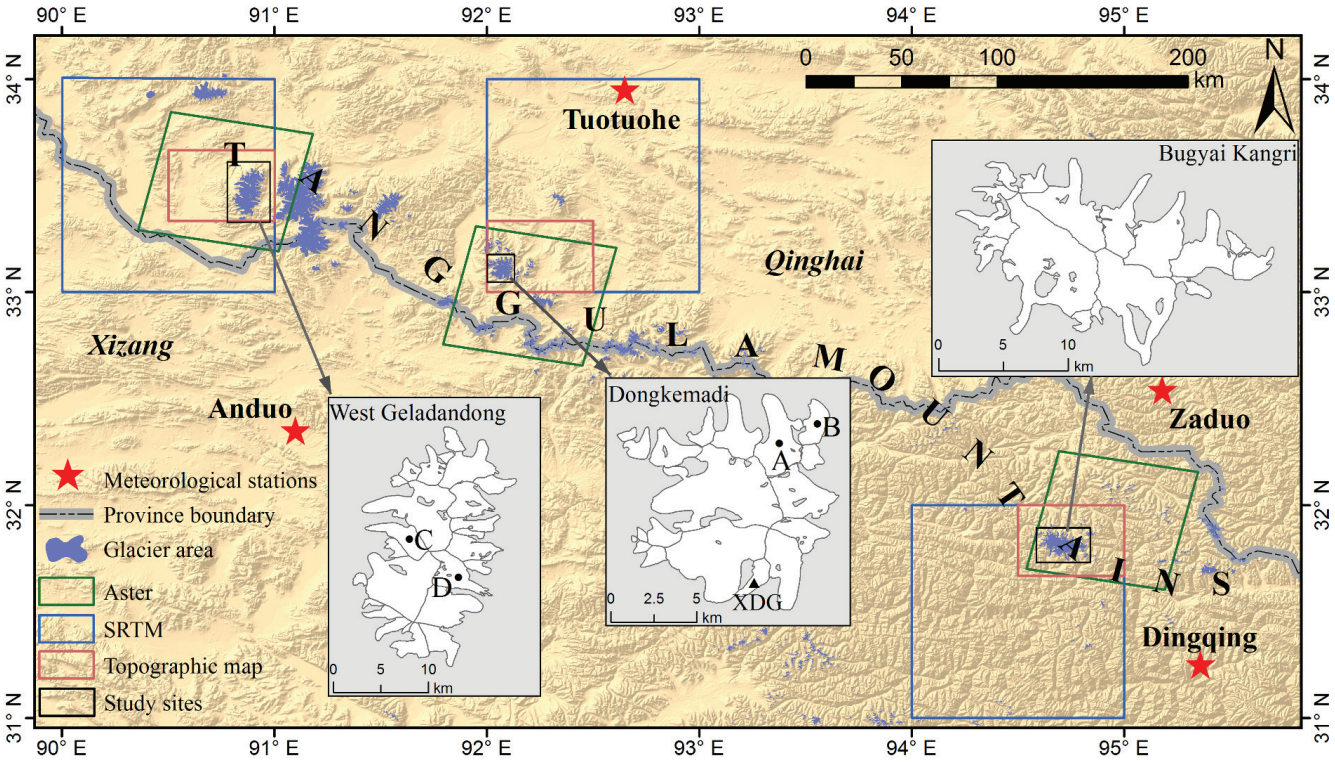

FIGURE 1. Sketch map of the Tanggula Mountains that shows the areas covered by the elevation data used in this study and the glacier boundaries covering the study sites based on Landsat TM images obtained in 2000. The background is a hillshade image derived from SRTM data, and the red stars indicate meteorological stations distributed around the Tanggula Mountains.

TABLE 1

Detailed information on the remote sensing data sets.

Sensor	Date*	ID	Spatial resolution	Coverage range
Landsat TM	22/09/1999	LT51360381999265BKT00	30 m	Bugyai Kangri
Landsat TM	12/04/1999	LT51380371999103BJC00	30 m	West-Geladandong
Landsat TM	30/08/2000	LT51370372000243BJC00	30 m	Dongkemadi
Landsat TM	22/02/2010	LT51380372010053BKT00	30 m	West-Geladandong
Landsat OLI	30/12/2015	LC81370372015364LGN00	15m	Dongkemadi
ASTER	11/02/2003	L1A_00302112003044645	15 m	Dongkemadi
ASTER	29/10/2007	L1A_00310292007043915	15 m	Dongkemadi
ASTER	21/02/2010	L1A_00302212010045147	15 m	West-Geladandong
ASTER	25/10/2014	L1A_00310252014043401	15 m	Bugyai Kangri
ASTER	29/12/2015	L1A_00312292015044606	15 m	Dongkemadi

*Dates given as dd/mm/yyyy.

veying and Mapping, 2007). The map-based DEMs (hereafter Topo DEM) were generated from the topographic maps using the ANUDEM5.23 software with a spatial resolution of 15 m. To compare the map with the SRTM data, the Topo DEMs were transformed to the WGS1984 UTM zone 46 coordinate system, and their spatial resolutions were resampled to 30 m.

SRTM

The SRTM DEM covers the region between 60°N and 56°S and is based on single-pass synthetic aperture radar interferometry (InSAR). Two antenna pairs, operating in the C-band (5.7 GHz) and X-band (9.7 GHz), simultaneously illuminated and recorded radar signals

during February 2000 (Farr et al., 2007). The SRTM1 (C-band) data with a spatial resolution of 30 m was used and acquired in February 2000. These data refer to the 1999 glacier surfaces at the end of the ablation season (Rignot et al., 2001). The vertical reference coordinate of the SRTM data set is the WGS84 EGM96 geoid (http://earthexplorer.usgs.gov/). The absolute vertical accuracy of the SRTM1 data sets is ±16 m, and the relative vertical accuracy is ±6 m (within 90% confidence) (Rabus et al., 2003).

ASTER Imagery

The ASTER sensor is part of the Terra satellite platform, and it provides multispectral imagery covering the Earth's surface between 82°N and 82°S. Stereo images from ASTER are suitable for DEM generation in mountainous terrain, and have been widely employed to assess changes in glacier volume and mass budget (Kääb, 2008; Bolch et al., 2011). In this study, we used Level 1A ASTER stereoscopic images to generate the DEMs. These images were acquired in February 2010, October 2014, and December 2015 for the West-Geladandong, Bugyai Kangri, and Dongkemadi sites, respectively, under small amounts of fresh snow and no cloud cover conditions. An ASTER DEM with a spatial resolution of 30 m was generated using the "DEM Extraction" module of ENVI 5.2, and the coordinate system was defined using the datum WGS1984 UTM zone 46. More than 300 randomly distributed points from the 1:100,000 topographic map were considered as ground control points.

Meteorological Data

The relationship between glacier mass budgets and climate variability was explored by analyzing summer temperatures and annual precipitation data measured at four meteorological stations distributed around the Tanggula Mountains (Fig. 1). The temperature and precipitation data from each station were provided by the Chinese National Meteorological Center (CNMC; http://data.cma.cn/site/index.html) (Table 2). We used the meteorological data from the four stations to represent the spatial and temporal variations in meteorological conditions across the study area.

DEM Coregistration and Accuracy

Planimetric and Vertical Adjustments of the DEMs

Previous studies have described a method for coregistering two DEMs based on the relationship between horizontal shifts and the corresponding slope and aspect values (Nuth and Kääb, 2011; Pieczonka et al., 2013). Here, the horizontal shift is determined by minimizing the root mean squared error of the elevation differences observed in glacier-free areas; the terrain is assumed to be stable over the study period. We chose the SRTM as the master DEM when coregistering the other DEMs. Table 3 lists the magnitude and direction of the shift vector between the master and slave DEMs. After the planimetric adjustment, the vertical bias between the DEMs can be adjusted by using the relationships between the elevation differences and the maximum curvature derived, for both glaciated and glacier-free areas (Gardelle et al., 2012).

Radar Penetration and Seasonality Correction

As the penetration depth of radar in snow and ice is directly affected by local climatic conditions, the degree to which measurements of glacier surface are underestimated varies regionally (Kääb et al., 2012; Gardelle et al., 2013). We compared available ICESat GLA14 footprints with SRTM elevation data in order to assess the penetration depth, following Kääb et al. (2012). As the SRTM data we used were acquired in February 2000, we selected footprints acquired around February. Footprints acquired in 2006 and 2008 were selected for West-

TABLE 2

Details of meteorological stations distributed around the Tanggula Mountains.

Station	Latitude (°N)	Longitude (°E)	Altitude (m a.s.l.)	Annual T. (°C)	Annual P. (mm)	Period covered
Dingqing	95.36	31.25	3873.1	3.5	649.3	1954–2016
Zaduo	95.18	32.54	4066.4	0.7	530.6	1956–2016
Tuotuohe	92.65	33.95	4533.1	–3.9	291.2	1956–2016
Anduo	91.1	32.35	4800.0	–2.5	444.8	1965–2016

Note: Annual T. and Annual P. are the means of annual temperature and annual precipitation from 1950s to 2016, respectively.

TABLE 3

Displacement vectors in X and Y directions between the master (SRTM) and slave DEMs.

Region	Item	Topo–SRTM	Aster–SRTM
Bugyai Kangri	X (m)	–10.28	–113.01
	Y (m)	–89.40	–1.45
Dongkemadi	X (m)	5.00	–8.80
	Y (m)	–14.35	76.10
West-Geladandong	X (m)	–58.05	–1.74
	Y (m)	–77.43	138.31

Note: positive values of X and Y indicate shifts to east and north, respectively; negative values of X and Y indicate shifts to west and south, respectively.

Geladandong, and footprints acquired in 2004 and 2008 were selected for Dongkemadi. Unfortunately, there were no useful ICESat tracks that crossed Bugyai Kangri. Therefore, we assumed a penetration depth of 2.5 ± 0.5 m, which corresponds to the mean of the penetration depth estimates for East Nepal and Bhutan given by Kääb et al. (2012). We eliminated the differences as a result of elevation changes that occurred between 2000 and when the ICESat data were acquired by assuming a linear rate of change.

The glaciers were divided into ablation and accumulation areas by the approximate mean value of the median elevation (Appendix Table A1). The median elevations in West-Geladandong and Dongkemadi were 5750 and 5600 m, respectively. The results in West-Geladandong showed a mean penetration depth of 0.3 ± 3.6 m for the glacier-free area, 1.1 ± 3.8 m for the ablation area, and 3.8 ± 5.0 m for the accumulation area. In the Dongkemadi region, the penetration depths were 0.1 ± 4.3 m for the glacier-free area, 3.7 ± 3.8 m for the ablation area, and 4.4 ± 2.7 m for the accumulation area, respectively. The mean values over the entire glacier-covered area in the two regions were 2.1 ± 4.5 m and 3.8 ± 3.5 m for West-Geladandong and Dongkemadi, respectively. The uncertainty about the penetration depth was evaluated by the standard error (Kääb et al., 2012).

The ASTER DEMs were acquired between October and February, and the SRTM DEM was obtained in February. Thus, we must be able to account for possible mass changes during this 1–5 month period in order to estimate the mass budget over an integer number of years. Glaciers in the Tanggula Mountains are the summer accumulation type (Fujita, 2008). Recent field observations indicated that no winter accumulation occurred on the XDG, and more than 90% of the precipitation occurred in summer over this mountain region (He et al., 2009). Thus, the seasonality correction was set to 0. For example, the ASTER image covering West-Geladandong was acquired in February 2010, and this image approximates the surfaces of glaciers it displays in 2009.

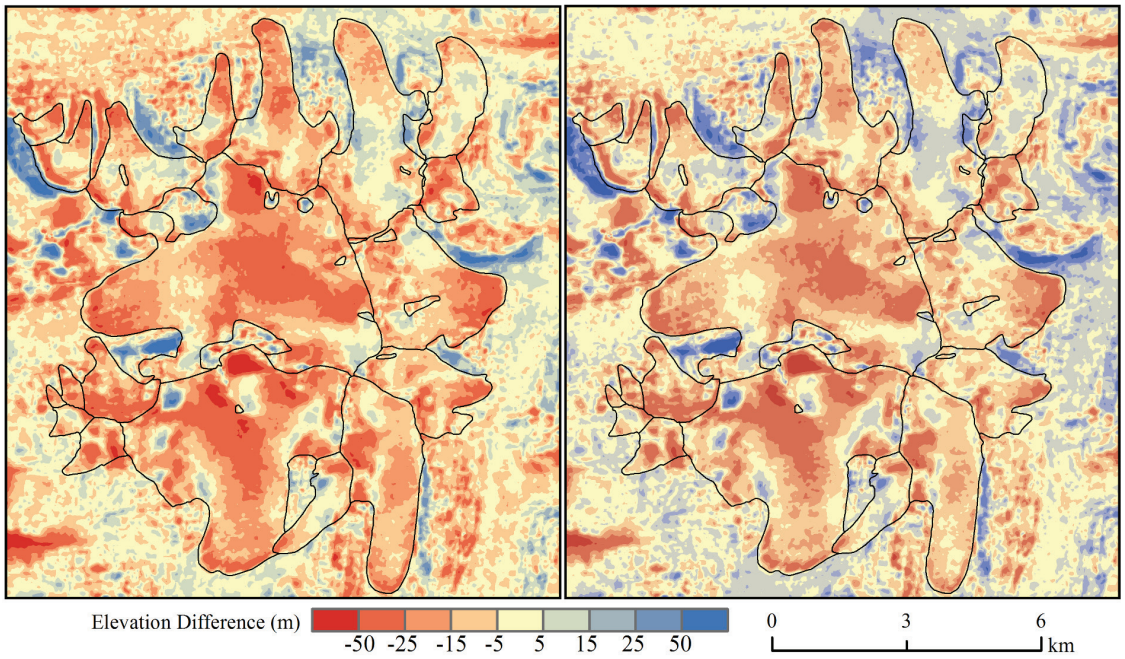

FIGURE 2. Elevation differences in the Dongkemadi region between 1969 (Topo DEM) and 2000 (SRTM), before (left) and after adjustment (right).

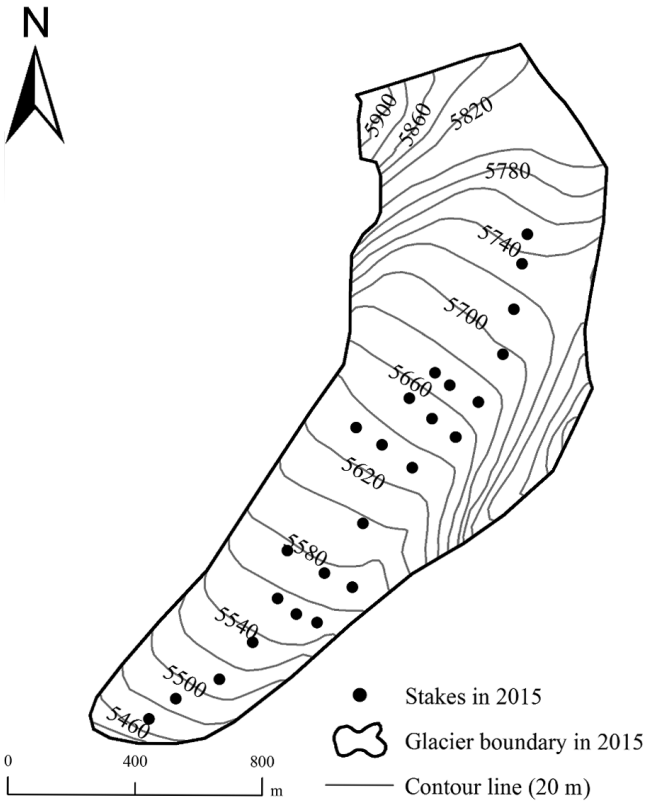

FIGURE 3. Stake network on the Xiao Dongkemadi glacier (XDG).

Accuracy Assessment

The relative uncertainties of DEMs prior to and after the adjustments were evaluated for non-glaciated terrain, which remained stable over the study period. Following Pieczonka et al. (2013), we set the 5% and 95% quartiles as the thresholds for eliminating outliers. The remaining pixels were employed to evaluate the uncertainties. The normalized median absolute deviation (NMAD; 1.482 × median $\left(\left|\tilde{x}-x_i\right|\right)$, where $\tilde{x}$ is the elevation difference and x_i is the median elevation difference), the radar wave penetration accuracy, the mean elevation difference (MED, Δh), and the uncertainty in the assumed density ($\Delta\rho$ = 60kg m^{-3}) were used to estimate the overall mass budget uncertainty. The NMAD is proportional to the median of the absolute differences between the errors and the median error (Höhle and Höhle, 2009). This metric provides a rather pessimistic assessment of the relative vertical accuracy (Kronenberg et al., 2016). The assumed density of 850 ± 60kg m^{-3} corresponds to the value suggested by Huss (2013). The uncertainty in the thickness changes (u_{DEM}) was calculated using Equation (1) considering the radar wave penetration accuracy (Δp) and the NMAD ($\Delta\sigma$) for the glacier-free terrain after DEM coregistration. The relative uncertainty between the Topo DEM and the ASTER DEM can be described directly by the NMAD because the DEMs are derived from optical images. The overall mass budget uncertainty (u_{M}) was estimated from Equation (2), where t is the time period, Δh is the MED of the glacier area, and ρ_{w} (1000kg m^{-3})and ρ_{I}(850kg m^{-3}) denote the densities of water and ice, respectively.

$$u_{DEM} = \sqrt{(\Delta\sigma)^2 + (\Delta p)^2} \tag{1}$$

$$u_M = \sqrt{\left(\frac{\Delta h}{t} \star \frac{\Delta\rho}{\rho W}\right)^2 + \left(\frac{u_{DEM}}{t} \star \frac{\rho I}{\rho W}\right)^2} \tag{2}$$

Glaciological Mass Balance Observations on the Xiao Dongkemadi Glacier

The mass balance of the XDG has been monitored since 1989. By 2015, 24 stakes had been set up on the surface of the glacier (Fig. 3), at sites ranging in elevation from 5400 m a.s.l. to 5750 m a.s.l. The net balance is obtained by measuring changes in stake heights and snow-pit features that occur in the ablation and accumulation areas. The measurements recorded at each stake include the height of the stake above the glacier surface, the density and thickness of the snow, the occurrence of superimposed ice layers, and the structure of the snow-pit profile (Pu et al., 2008). The mass balance b at each stake and in each snow pit can be calculated as follows:

$$b = \Delta S \times \rho_S + \Delta I \times \rho_I \tag{3}$$

where ΔS and ΔI denote changes in snow and ice layer thickness, and ρ_{S} and ρ_{I} denote the densities of snow and ice, respectively.

The mass balance at each stake is assigned to a corresponding altitude range, and the specific mass balance is depicted as a function of altitude. These data are then extrapolated to the whole glacier. The total mass balance B can be calculated as follows:

$$B = \frac{\sum S_n \times b_n}{S}, \tag{4}$$

where S is the total area of the glacier, and S_{n} and b_{n} are the area and specific mass balance of each altitudinal range, respectively.

TABLE 4

Statistics of the original and adjusted relative uncertainties between the Topo, SRTM, and ASTER DEMs in the three subregions.

		Original		Adjusted			
Regions	Item	MED (m)	STDEV	MED (m)	STDEV	NMAD	u_{DEM}(m)
Bugyai Kangri	Topo-SRTM	–13.7	32.7	–0.9	32.6	3.1	3.2
	Aster-SRTM	–61.3	35.4	2.6	35.4	4.2	4.3
	Aster-Topo	–78.2	40.8	3.3	38.4	2.8	2.8
Dongkemadi	Topo-SRTM	–3.5	12.2	0.3	11.8	1.0	3.6
	Aster-SRTM	–56.9	12.3	–0.1	12.2	1.3	3.7
	Aster-Topo	–60.3	16.9	0.2	16.4	1.3	1.3
West-Geladandong	Topo-SRTM	–12.3	27.3	0.5	27.2	3.2	5.5
	Aster-SRTM	–67.6	16.0	–0.2	9.3	1.8	4.8
	Aster-Topo	–79.9	29.1	0.6	28.9	2.7	2.7

Note: MED is mean elevation difference; STDEV is standard deviation; NMAD is the normalized median absolute deviation.

RESULTS

Validation between Glaciological and Geodetic Results

The results of both glaciological and geodetic methods indicated significant mass loss from the XDG for the period 1999–2015 (Table 5). The changes in the specific mass budget determined using the geodetic method agreed with the glaciological results for the different periods between 1999 and 2015. The absolute differences in mass budgets between the two methods were <5% for the periods 1999–2002, 1999–2007, and 1999–2015. The low absolute differences seen during many of these periods indicated that the mass budget estimated by geodetic methods compared favorably with the glaciological results. The lower uncertainty suggested increased confidence in the mass budgets estimated using the geodetic method.

Mass Budgets for the Entire Tanggula Mountains

Before averaging elevation changes, we excluded all elevation differences exceeding ±100 m in order to identify the largest realistic glacier elevation changes. Between ~1969 and ~2015, a significant surface lowering of 0.36 ± 0.06 m a^{-1} occurred within the entire Tanggula Mountains (Fig. 4 and Table 6). This downwasting resulted in an average surface lowering of 0.27 ± 0.14 m a^{-1} between ~1969 and 1999 (Fig. 5). This rate of downwasting was lower than that observed in 1999–2015, when the rate of surface lowering was 0.60 ± 0.35 m a^{-1} (Fig. 6). The overall specific mass budgets of entire Tanggula Mountains for the periods ~1969 to ~2015, ~1969 to 1999, and 1999 to ~2015 were –0.31 ± 0.05, –0.23 ± 0.12, and –0.51 ± 0.30 m w.e. a^{-1}, respectively.

Between ~1969 and ~2015, West-Geladandong experienced the lowest specific mass loss of 0.22 ± 0.06 m w.e. a^{-1}, and Dongkemadi and Bugyai Kangri showed

TABLE 5

Mass budgets calculated using the two methods for the XDG during 1999–2015.

Period	Glaciological results (m w.e. a^{-1})	Geodetic results (m w.e. a^{-1})	Absolute diff. (%)
1999–2003	–0.30	–0.29 ± 0.79	1.9
1999–2007	–0.38	–0.36 ± 0.33	4.5
1999–2015	–0.42	–0.41 ± 0.21	1.2

Note: The absolute diff. is the absolute difference for mass balance results, calculated from the two methods, with the uncertainty excluded from the geodetic method value.

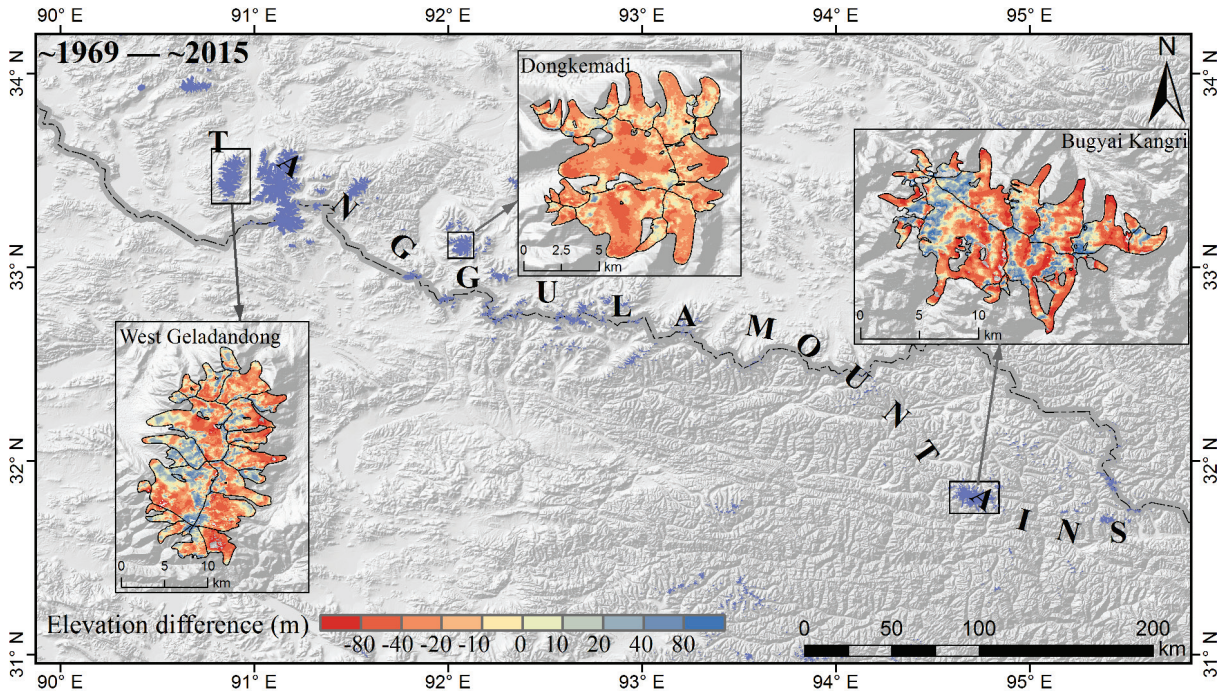

FIGURE 4. Glacier surface elevation differences between ~1969 and ~2015.

TABLE 6

Glacier mass budgets and surface elevation changes for each subregion in the Tanggula Mountains.

		~1969 to 1999		1999 to ~2015		~1969 to ~2015	
Region	Glacier area (km^2)	MED ($m\ a^{-1}$)	SMB ($m\ w.e.\ a^{-1}$)	MED ($m\ a^{-1}$)	SMB ($m\ w.e.\ a^{-1}$)	MED ($m\ a^{-1}$)	SMB ($m\ w.e.\ a^{-1}$)
Bugyai Kangri	130.5	–0.31±0.10	–0.26±0.09	–0.74±0.28	–0.63±0.25	–0.44±0.06	–0.37±0.06
Dongkemadi	73.6	–0.25±0.12	–0.21±0.10	–0.87±0.23	–0.74±0.21	–0.46±0.06	–0.39±0.04
West Geladandong	178.4	–0.25±0.18	–0.21±0.16	–0.39±0.44	–0.33±0.38	–0.26±0.06	–0.22±0.06
Total/average	382.5	–0.27±0.14	–0.23±0.12	–0.60±0.35	–0.51±0.30	–0.36±0.06	–0.31±0.05

Note: MED is mean elevation difference; SMB is specific mass balance.

similar mass losses of 0.39 ± 0.04 and 0.37 ± 0.06 m w.e. a^{-1}, respectively. For the period ~1969–1999, the greatest mass loss was 0.26 ± 0.09 m w.e. a^{-1} in Bugyai Kangri, which was slightly greater than that noted in Dongkemadi (0.21 ± 0.10 m w.e. a^{-1}) and West-Geladandong (0.21 ± 0.16 m w.e. a^{-1}). Continuous mass loss occurred in the entire Tanggula Mountains between 1999 and ~2015. The mass losses in Dongkemadi (0.74 ± 0.21 m w.e. a^{-1}) and Bugyai Kangri (0.63 ± 0.25 m w.e. a^{-1}) were larger than that those noted in West-Geladandong (0.33 ± 0.38 m w.e. a^{-1}) from 1999 to ~2015. The relatively low mass loss in West-Geladandong might reflected the different time periods considered for each region; however, no ASTER scenes were available after 2010 for West-Geladandong. The glaciers in the Tanggula Mountains experienced accelerating mass loss during the period 1999 to ~2015, compared with the previous period (~1969–1999).

Discussion

Existing studies of glacier changes in the Tanggula Mountains indicated overall glacier shrinkage. During the past 30 years, the glaciers in the eastern and central parts of the Tanggula Mountains shrank by 15.3% and 22.2%, respectively (Liu et al., 2016; Wang et al., 2016). However, the relatively large glaciers in the Dongkemadi and Geladandong regions shrank by less than 5% between 1969 and the early 21st century (Ye et al., 2006; Li et al., 2012). Continuous reductions in surface eleva-

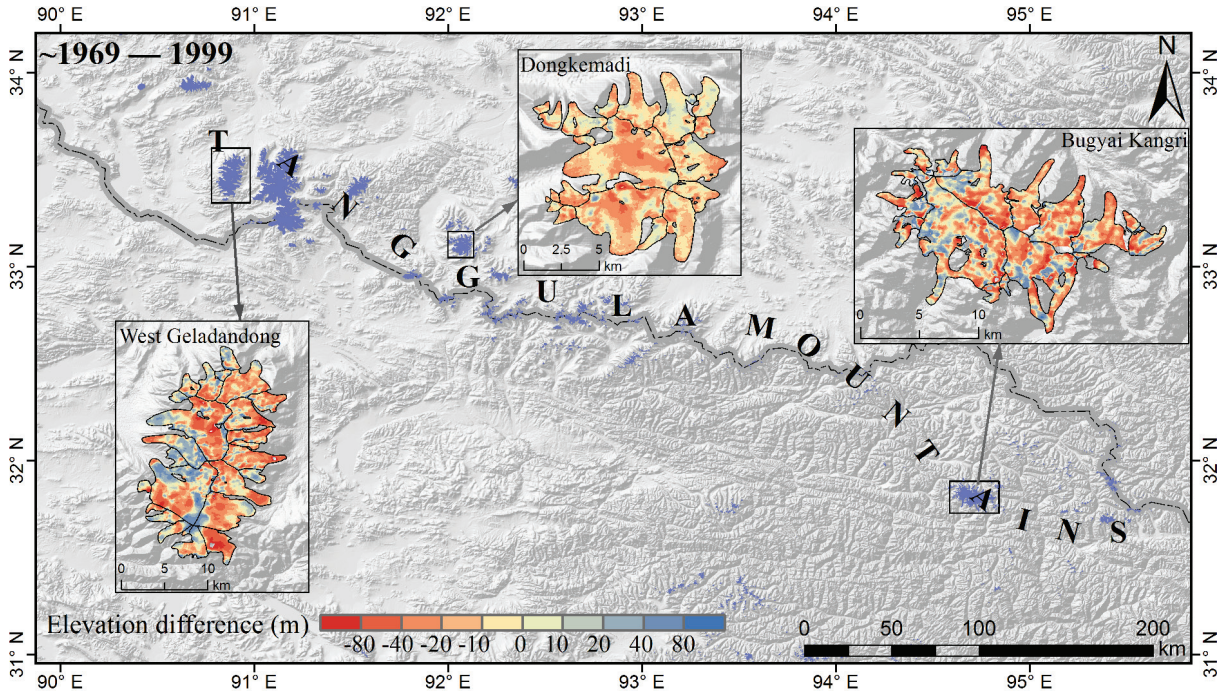

FIGURE 5. Glacier surface elevation differences between ~1969 and 1999.

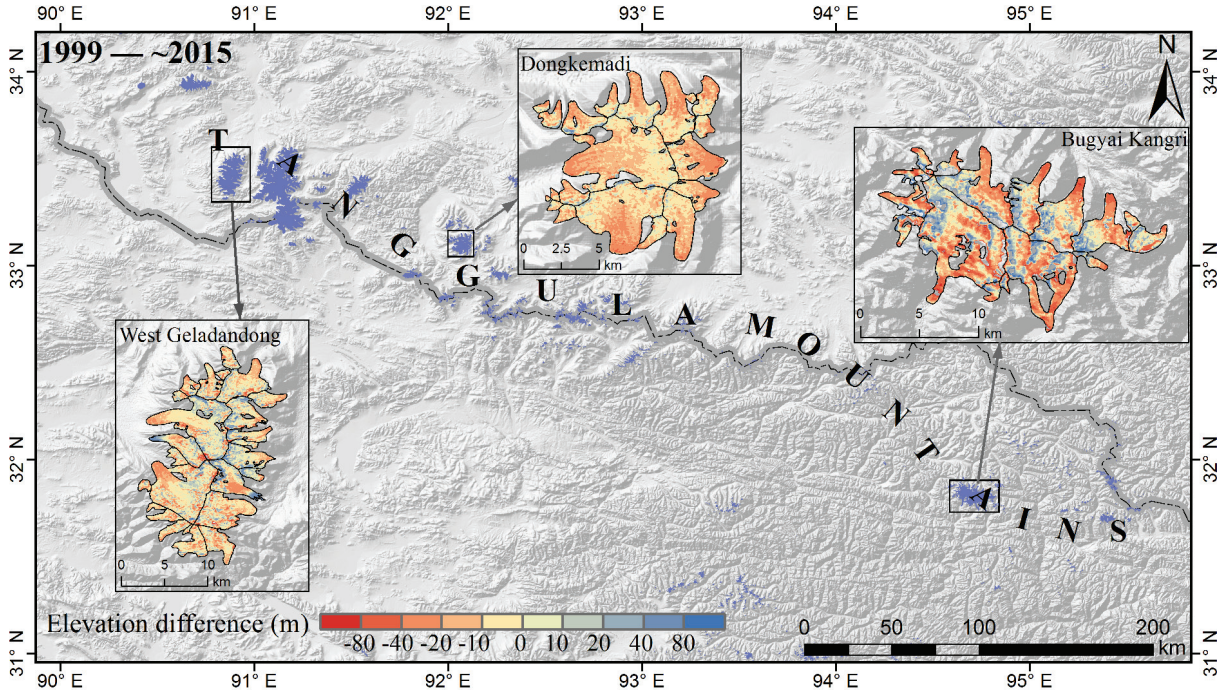

FIGURE 6. Glacier surface elevation differences between 1999 and ~2015.

tion of 12.6 ± 6 m and 3.4 m occurred in the Dongkemadi region for the periods 1969–2000 and 2003–2008, respectively (Li et al., 2012; Ke et al., 2015b). Considering the penetration of C-band single beam radar at Dongkemadi (3.8 ± 3.5 m), our result (–7.4 ± 3.6 m) agreed with that of Li et al. (2012) (12.6 ± 6 m).

Although glaciological and geodetic methods represent two recognized means of calculating mass budgets, the mass budgets calculated using glaciological (–0.54 m w.e. a^{-1}) and geodetic (–0.81 m w.e. a^{-1}) methods showed significant discrepancies on a global scale during the first decade of the 21st century. This discrepancy might be

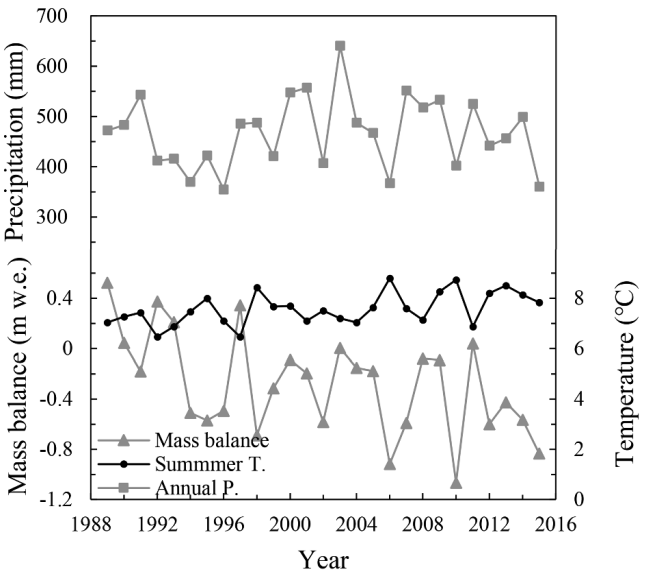

FIGURE 7. Variations in the mass balance of the XDG and summer temperature and annual precipitation at Anduo station from 1989 to 2015.

attributed to the number of glaciers considered and the conversion density, rather than a systematic difference between the two methods (Zemp et al., 2015). A widely used conversion density of 850 ± 60 kg m^{-3}, which was proposed by Huss (2013), had been applied in many regions (Shangguan et al., 2015; Bolch et al., 2017).

The satisfactory verification of mass budget calculations for the XDG obtained in this study indicated that the geodetic method was an accurate and credible method for calculating glacier mass budgets, compared with glaciological results. Ke et al. (2015b) calculated a specific mass budget of −0.42 ± 0.08 m w.e. a^{-1} in the Dongkemadi region between 2003 and 2008 using ICESat data and employing a conversion density of 750 kg m^{-3}. However, adjusting these results using the standard conversion density (850 ± 60 kg m^{-3}) produces a mass budget of approximately −0.48 ± 0.09 m w.e. a^{-1}, which was less than the value of −0.74 ± 0.21 m w.e. a^{-1} for 1999–2015 calculated in this study. There were two possible reasons for the discrepancy between these two studies. On the one hand, the ICESat footprint only extended across the eastern part of the Dongkemadi region, meaning that the use of the mass budget of the eastern part to represent the entire region may lead to biased results. On the other hand, the time span of the present study was 10-year longer than the ICESat time series, and the trend towards mass loss accelerated at the XDG after 2010 (Fig. 7).

Regional mass-balance estimates are required to assess the contributions of glacier changes to hydrological processes. In most studies, the average mass balance of the glaciers monitored was generally selected to represent the regional value (Yao et al., 2012; Zemp et al., 2013). In the Tanggula Mountains, there is only one long-term monitored glacier (the XDG), which occupies an elevation range of 5376–5910 m. Using the mass budget of the XDG to represent the regional value will therefore result in an underestimation of mass loss (Table 7). The mass budget measured using the glaciological method at the XDG cannot cover the entire study area, particularly low-altitude areas (the termini of some glaciers are lower than 5400 m; Appendix Table A1) that experience high ablation. ICESat altimetry data are valuable for estimating large-scale mass budgets (Gardner et al., 2013). For medium and small scales, the regional mass budget calculated from ICESat depends on the selected scales and the locations of the footprints (Neckel et al., 2014; Ke et al., 2015b). Compared with the mass budgets calculated using the glaciological method and ICESat altimetry, the multi-temporal DEMs used in the present study can provide a more representative estimate of the regional mass budget because they cover entire mountain ranges.

Glacier mass budgets are sensitive to climate change, and the glaciological method provides a high-resolution mass balance for studying glacier–climate interactions. The annual mass balance of the XDG and the summer temperature and annual precipitation measured at Anduo station between 1989 and 2015 are shown in Figure 7. The variations in mass loss showed a positive relationship with summer temperature (correlation coefficient of 0.79; $p < 0.01$) and a negative relationship with annual precipitation (correlation coefficient of –0.40; $p <$

TABLE 7

Mass budgets of the XDG, the Dongkemadi region, and the Tanggula Mountains during different periods.

Period	Xiao Dongkemadi (m w.e. a^{-1})	Dongkemadi region (m w.e. a^{-1})	Tanggula Mountains (m w.e. a^{-1})
1969–1999	–0.06 ± 0.10	–0.21 ± 0.10	–0.23 ± 0.12
1999–2015	–0.41 ± 0.21	–0.74 ± 0.21	–0.51 ± 0.30
1969–2015	–0.17 ± 0.04	–0.39 ± 0.04	–0.31 ± 0.05

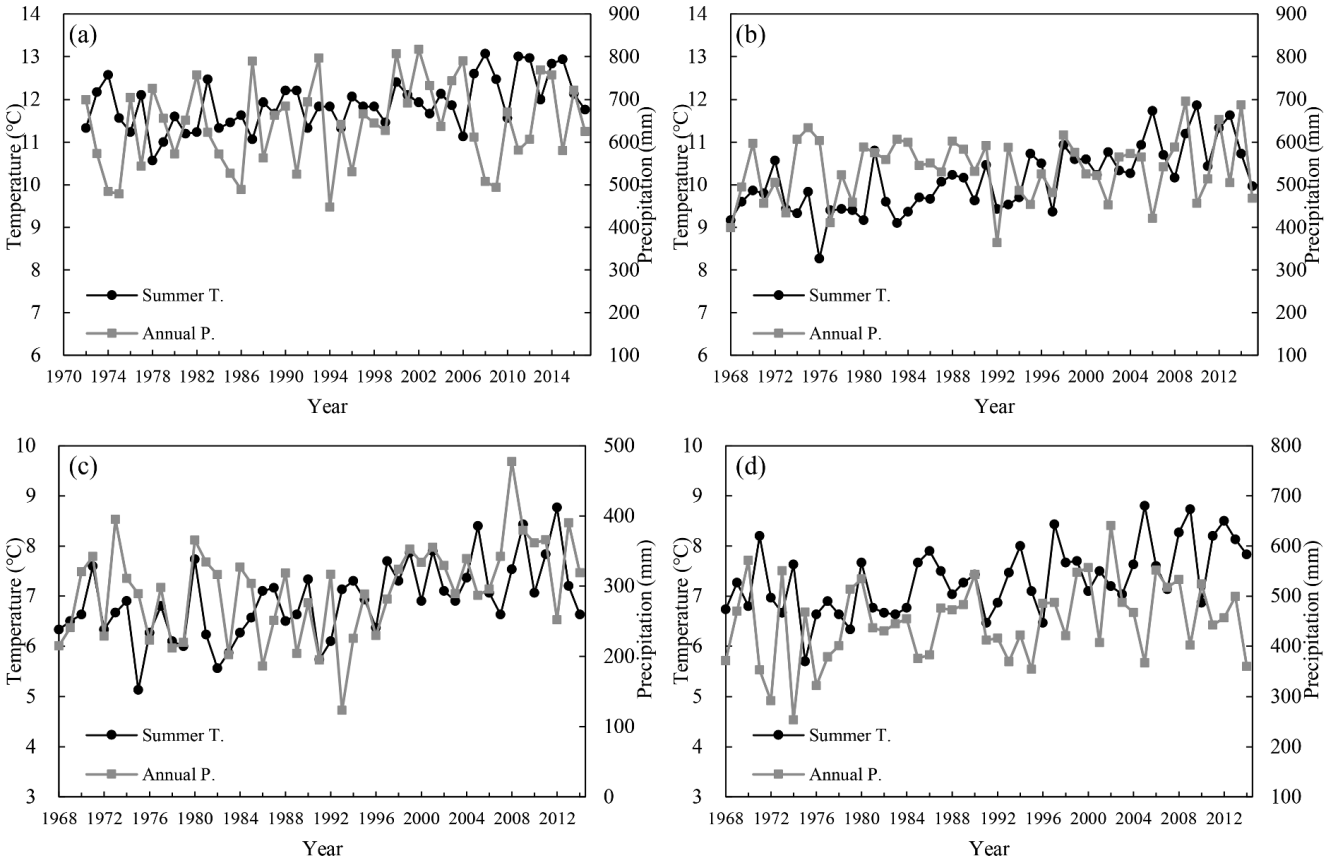

FIGURE 8. Summer temperature and annual precipitation measured at the meteorological stations around the Tanggula Mountains between ~1969 and 2015: (a) Dingqing, (the meteorological data for 1969 are missing); (b) Zaduo; (c) Tuotuohe; and (d) Anduo.

TABLE 8

Variations in summer temperature and annual precipitation around the Tanggula Mountains for the periods ~1969–1999, 1999–2015, and ~1969–2015.

Station	Temperature (°C 10a^{-1})			Precipitation (% 10a^{-1})		
(slope)	1969–1999	1999–2015	1969–2015	1969–1999	1999–2015	1969–2015
Dingqing (S)	0.13	0.41	0.22**	3.7	–7.3	2.4
Anduo (S)	0.20	0.55	0.27**	2.2	–13.4	3.6
Zaduo (N)	0.27*	0.28	0.38**	1.8	1.7	1.5
Tuotuohe (N)	0.18	0.07	0.30**	–4.8	3.2	6.0

Note: * within 95% confidence; ** within 99% confidence.

0.05). Increases in summer temperature (0.4 °C 10a^{-1}, as determined by linear fitting) and fluctuations in annual precipitation (which contains a weak trend of –1.3% 10a^{-1}, as determined by linear fitting) resulted in the observed continuous mass loss from the XDG from 1989 to 2015.

The changes in the mass budget likely resulted from a combination of changes in temperature and precipitation (Wang et al., 2010; Wiltshire, 2014). The summer temperature and annual precipitation around the Tanggula Mountains varied among the different regions and periods of time (Fig. 8). The Dingqing and Zaduo stations are located in the eastern region of the Tanggula Mountains, while the Tuotuohe and Anduo stations are located in the western region (Fig. 1). The linear fits of summer temperature and annual precipitation at

the four stations during different periods are listed in Table 8. Over 1969–2015, the annual precipitation in the Tanggula Mountains increased slightly at rates ranging from 1.5% to 6% $10a^{-1}$, and significant increases in summer temperatures of 0.22–0.38 °C $10a^{-1}$ were noted. Between 1969–1999 and 1999–2015, accelerated increases in summer temperatures occurred on the southern slopes, whereas similar or lower values were found on the northern slopes. The amount of precipitation that fell on the southern slopes decreased sharply in 1999–2015, reversing the slow increase that occurred from 1969 to 1999; however, precipitation changed only slowly on the northern slopes.

Oerlemans (2005) revealed that the effects of a 1 °C warming on the mass budget of a glacier is equivalent to that of a 25% increase in precipitation. Between 1969 and 2015, increase in temperature and slight precipitation changes resulted in the continuous mass loss in the Tanggula Mountains. Over 1999–2015, the large observed rates of temperature increase and the heterogeneous precipitation changes (which reflected decreases at Dingqing and Anduo, no change at Zaduo, and an increase at Tuotuohe) caused the overall accelerated mass loss compared to the period ~1969–1999.

The formation and expansion of proglacial lakes can affect the retreats of individual glaciers (Sakai et al., 2009; Gardelle et al., 2011). The lake-terminating glaciers in Bugyai Kangri had retreated more rapidly than the land-terminating glaciers within the same region (Liu et al., 2016). Proglacial lakes enhanced the glacier mass losses because of calving (Bolch et al., 2011). In the Dongkemadi region, the mass budget was comparable at glaciers A and B during all of the investigated periods (Fig. 1 and Appendix Table A2). However, the terminus of glacier A was 100 m lower than that of glacier B, and glacier A was more than twice the size of glacier B (Table A1). Large glaciers with low terminal elevations experienced greater mass losses than small glaciers with termini at high elevations (Wei et al., 2015), meaning that the mass loss of glacier A would be greater than that of B. The discrepancy between the measurements and the observations can be attributed in part to the expansion of a proglacial lake at the terminus of glacier B (Fig. 9). The lake formed after 1969 and grew significantly between 2000 and 2015 (Fig. 9). The rapid growth of the proglacial lake increases the risk of outburst flood hazards in the Tanggula Mountains.

The two advancing glaciers in West-Geladandong, glaciers C and D (Fig. 1), showed positive surface elevation changes of 2.9 ± 4.2 m and 6.6 ± 4.2 m between 1999 and 2009, respectively. Hence, we examined the changes at the glacier boundaries using Landsat TM images. Two images from 1999 and 2010 showed an obvious advance and increase in the areas covered by glaciers C and D (Fig. 10, parts c and d). These results agreed with the increase in the surface elevations of the two glaciers from 1999 to 2009. Distinct areas of mass loss and gain could be recognized on glaciers C and D: significant mass gains were measured in the glacier tongue regions, while clear mass losses occurred in the middle parts of these glaciers, and slight mass gains were noted the upper parts of the glaciers (Fig. 10, part a). These area changes and patterns of elevation change may indicate that glaciers C and D are surge-type glaciers.

The total mass budget for the entire Tanggula Mountains between ~1969 and ~2015 (–0.31 ± 0.05 m w.e. a^{-1}) was similar to that reported for several other regions around the Tibetan Plateau, including the Ne-

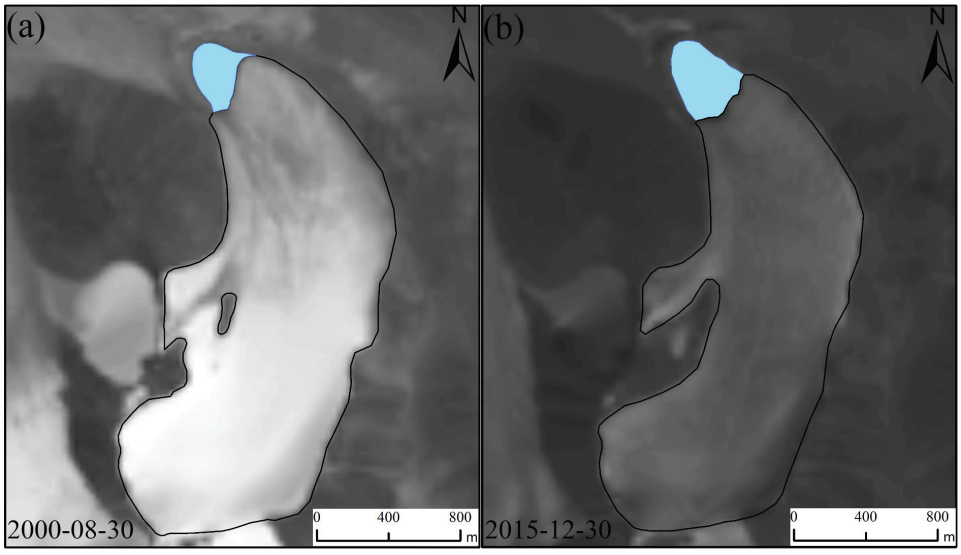

FIGURE 9. Proglacial lake (blue) derived from Landsat images. (a) Proglacial lake in 2000 with an area of 0.07 km^2, and (b) proglacial lake in 2015 with an area of 0.12 km^2.

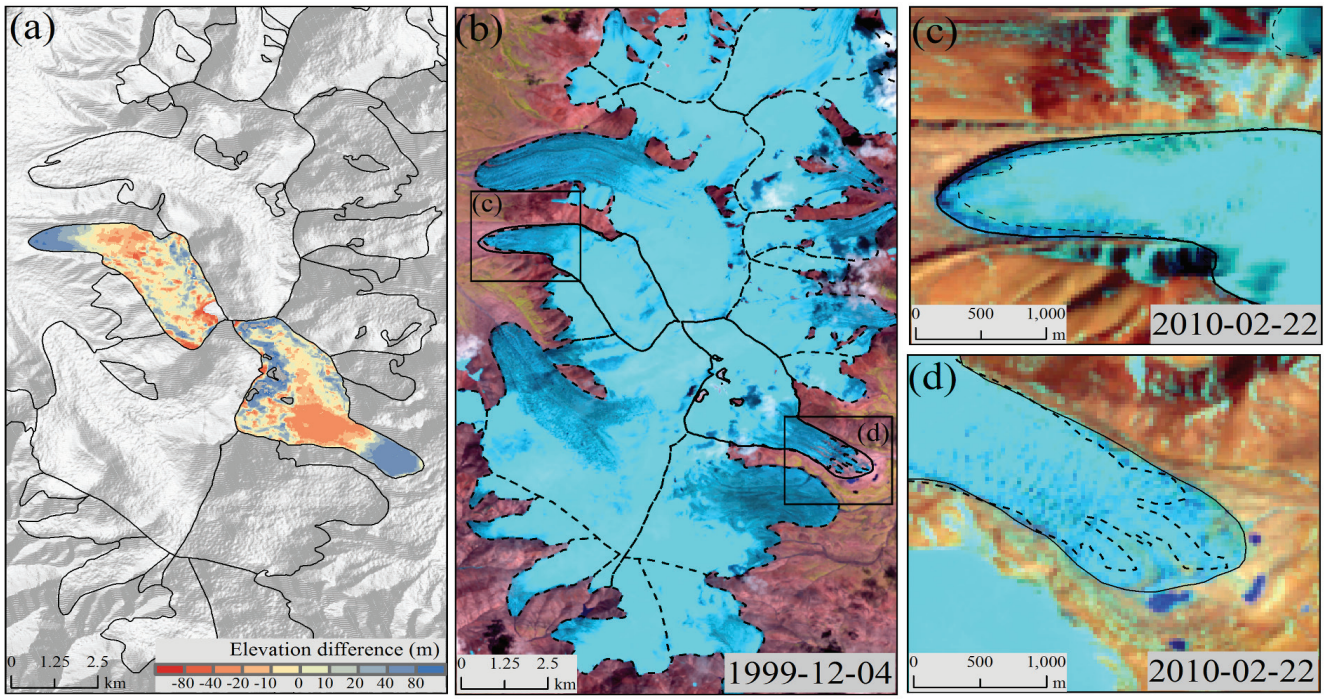

FIGURE 10. (a) Elevation differences between ASTER (2009) and SRTM (1999) images for glaciers C and D; (b) Landsat TM from 1999 showing the 1999 glacier boundary (dashed line) and the 2010 glacier boundary (solid line); (c) 2010 Landsat TM image for glacier C; and (d) 2010 Landsat TM image for glacier D.

pal Himalayas (-0.32 ± 0.08 m w.e. a^{-1} for 1970–2007; Bolch et al., 2011) and the Aksu–Tarim catchment (-0.33 ± 0.15 m w.e. a^{-1} for 1976–2009; Pieczonka et al., 2013), but was lower than that in the Chinese Altai Mountains (-0.43 ± 0.03 m w.e. a^{-1} for 1958–2008; Wei et al., 2015), as well as the average value determined from 37 reference glaciers worldwide (−0.40 m w.e. a^{-1} for 1980–2011; Zemp et al., 2013). The mass budget changes determined for the studied glacier were -0.23 ± 0.12 m w.e. a^{-1} for ~1969–1999 and -0.51 ± 0.30 m w.e. a^{-1} for 1999 to ~2015, and indicated accelerated mass losses in the Tanggula Mountains in the recent decade.

Conclusions

Multi-temporal DEMs provide a spatially representative resource for estimating regional mass budgets. This study presents mass budgets derived by the geodetic method for the entire Tanggula Mountains over the past four decades. The glaciological and geodetic methods yielded similar mass budget estimates for the XDG for 1999–2015. Continuous mass loss in the Tanggula Mountains has been measured since ~1969. The glacier mass budgets were negative for the period ~1969–1999 (-0.23 ± 0.12 m w.e. a^{-1}), and an accelerated mass loss of 0.51 ± 0.30 m w.e. a^{-1} has been measured in recent years. Between ~1969 and ~2015, the mass budget calculated using the geodetic method for the entire Tanggula Mountains (-0.31 ± 0.05 m w.e. a^{-1}) was lower than the global average value derived from glaciological observations.

Heterogeneous glacier behavior is caused by a range of factors, including meteorological conditions, the development of proglacial lakes, and surge-type glacier behavior. Glaciers C and D experienced mass gains since 1999, and significant transfers of mass from the middle parts to the lower parts of these glaciers indicated that they were surge-type glaciers. Although the accelerated mass loss in the Tanggula Mountains was caused mainly by increases in summer temperatures, the formation and expansion of proglacial lakes would enhance the mass losses from glaciers. The rapid growth of proglacial lakes in the Tanggula Mountains should be monitored carefully.

Acknowledgments

This work was supported by the National Natural Science Foundation of China (Grants Nos. 41571076, 41501069), the Chinese MOST Basic Work Project (Grant No. 2013FY111400), and The Natural Science Fund for Colleges and Universities in Jiangsu Province

(Grant No. 15KJB170007). We gratefully acknowledge the contributors of the remote sensing data and their efforts in constructing the image database used in this study. Special thanks are given to two anonymous reviewers and the journal editor for critical comments on this manuscript.

References Cited

Arendt, A., Bolch, T., Cogley, J. G., Gardner, A., Hagen, J. O., Hock, R., Kaser, G., Pfeffer, W. T., Moholdt, G., and Paul, F., 2015: Randolph Glacier Inventory [v5. 0]: A Dataset of Global Glacier Outlines. Global Land Ice Measurements from Space, Boulder, Colorado, USA.

Bolch, T., Buchroithner, M., Pieczonka, T., and Kunert, A., 2008: Planimetric and volumetric glacier changes in the Khumbu Himal, Nepal, since 1962 using Corona, Landsat TM and ASTER data. *Journal of Glaciology*, 54(187): 592–600(599), doi: http://dx.doi.org/10.3189/002214308786570782.

Bolch, T., Pieczonka, T., and Benn, D. I., 2011: Multi-decadal mass loss of glaciers in the Everest area (Nepal Himalaya) derived from stereo imagery. *The Cryosphere*, 5(2): 349–358, doi: http://dx.doi.org/10.5194/tc-5-349-2011.

Bolch, T., Pieczonka, T., Mukherjee, K., and Shea, J., 2017: Brief communication: Glaciers in the Hunza catchment (Karakoram) have been nearly in balance since the 1970s. *The Cryosphere*, 11(1): 531–539, doi: http://dx.doi.org/10.5194/tc-11-531-2017.

Farr, T. G., Rosen, P. A., Caro, E., Crippen, R., Duren, R., Hensley, S., Kobrick, M., Paller, M., Rodriguez, E., and Roth, L., 2007: The Shuttle Radar Topography Mission. *Reviews of Geophysics*, 45(2): 33, doi: http://dx.doi.org/10.1029/2005RG000183.

Fujita, K., 2008: Effect of precipitation seasonality on climatic sensitivity of glacier mass balance. *Earth & Planetary Science Letters*, 276(1-2): 14–19, doi: http://dx.doi.org/10.1016/j.epsl.2008.08.028.

Fujita, K., and Ageta, Y., 2000: Effect of summer accumulation on glacier mass balance on the Tibetan Plateau revealed by mass-balance model. *Journal of Glaciology*, 46(153): 244–252, doi: https://doi.org/10.3189/172756500781832945.

Gao, H. K., He, X. B., Ye, B. S., and Pu, J. C., 2012: Modeling the runoff and glacier mass balance in a small watershed on the Central Tibetan Plateau, China, from 1955 to 2008. *Hydrological Processes*, 26(11): 1593–1603, doi: http://dx.doi.org/10.1002/hyp.8256.

Gardelle, J., Arnaud, Y., and Berthier, E., 2011: Contrasted evolution of glacial lakes along the Hindu Kush Himalaya mountain range between 1990 and 2009. *Global & Planetary Change*, 75(1-2): 47–55, doi: http://dx.doi.org/10.1016/j.gloplacha.2010.10.003.

Gardelle, J., Berthier, E., and Arnaud, Y., 2012: Impact of resolution and radar penetration on glacier elevation changes computed from DEM differencing. *Journal of Glaciology*, 58(208): 419–422, doi: http://dx.doi.org/10.3189/2012JoG11J175.

Gardelle, J., Berthier, E., Arnaud, Y., and Kääb, A., 2013: Region-wide glacier mass balances over the Pamir-Karakoram-Himalaya during 1999–2011. *The Cryosphere*, 7(4): 1263–1286, doi: http://dx.doi.org/10.5194/tc-7-1263-2013.

Gardner, A. S., Moholdt, G., Cogley, J. G., Wouters, B., Arendt, A. A., Wahr, J., Berthier, E., Hock, R., Pfeffer, W. T., and Kaser, G., 2013: A reconciled estimate of glacier contributions to sea level rise: 2003 to 2009. *Science*, 340(6134): 852, doi: http://dx.doi.org/10.1126/science.1234532.

He, X. B., Ye, B. S., and Ding, Y. J., 2009: Bias correction for precipitation mesuament in Tanggula Mountain Tibetan Plateau. *Advances in Water Science*, 20(3): 403–408, doi: http://dx.doi.org/10.14042/j.cnki.32.1309.2009.03.010 (in Chinese).

Höhle, J., and Höhle, M., 2009: Accuracy assessment of digital elevation models by means of robust statistical methods. *ISPRS Journal of Photogrammetry & Remote Sensing*, 64(4): 398–406, doi: http://dx.doi.org/10.1016/j.isprsjprs.2009.02.003.

Huang, L., Li, Z., Tian, B. S., Chen, Q., and Zhou, J. M., 2013: Monitoring glacier zones and snow/firn line changes in the Qinghai–Tibetan Plateau using C-band SAR imagery. *Remote Sensing of Environment*, 137(10): 17–30, doi: http://dx.doi.org/10.1016/j.rse.2013.05.016.

Huss, M., 2013: Density assumptions for converting geodetic glacier volume change to mass change. *The Cryosphere*, 7(7): 877–887, doi: http://dx.doi.org/10.5194/tc-7-877-2013.

Immerzeel, W. W., Beek, L. P. H. V., and Bierkens, M. F. P., 2010: Climate change will affect the Asian water towers. *Science*, 328(5984): 1382–1385, doi: http://dx.doi.org/10.1126/science.1183188.

Kääb, A., 2008: Glacier volume changes using ASTER satellite stereo and ICESat GLAS laser altimetry. a test study on Edgeøya, eastern Svalbard. *IEEE Transactions on Geoscience & Remote Sensing*, 46(10): 2823–2830, doi: http://dx.doi.org/10.1109/TGRS.2008.2000627.

Kääb, A., Berthier, E., Nuth, C., Gardelle, J., and Arnaud, Y., 2012: Contrasting patterns of early twenty-first-century glacier mass change in the Himalayas. *Nature*, 488(7412): 495–498, doi: http://dx.doi.org/10.1038/nature11324.

Kaser, G., Grosshauser, M., and Marzeion, B., 2010: Contribution potential of glaciers to water availability in different climate regimes. *Proceedings of the National Academy of Sciences of the United States of America*, 107(47): 20223–20227, doi: http://dx.doi.org/10.1073/pnas.1008162107.

Ke, L. H., Ding, X. L., and Song, C. Q., 2015a: Heterogeneous changes of glaciers over the western Kunlun Mountains based on ICESat and Landsat-8 derived glacier inventory. *Remote Sensing of Environment*, 168: 13–23, doi: http://dx.doi.org/10.1016/j.rse.2015.06.019.

Ke, L. H., Ding, X. L., and Song, C. Q., 2015b: Estimation of mass balance of Dongkemadi glaciers with multiple methods based on multi-mission satellite data. *Quaternary International*, 371: 58–66, doi: http://dx.doi.org/10.1016/j.quaint.2015.02.043.

Kronenberg, M., Barandun, M., Hoelzle, M., Huss, M., Farinotti, D., Azisov, E., Usubaliev, R., Gafurov, A., Petrakov, D., and Kääb, A., 2016: Mass-balance reconstruction for Glacier No. 354, Tien Shan, from 2003 to 2014. *Annals of Glaciology*, 57(71): 92–102, doi: http://dx.doi.org/10.3189/2016AoG71A032.

Li, X. Y., Ding, Y. J., Yu, Z. B., Mika, S., Liu, S. Y., Shangguan, D. H, and Lu, C., 2015: An 80-year summer temperature history from the Xiao Dongkemadi ice core in the central Tibetan Plateau and its association with atmospheric circulation. *Journal of Asian Earth Sciences*, 98: 285–295, doi: http://dx.doi.org/10.1016/j.jseaes.2014.09.025.

Li, X. Y., He, X. B., Kang, S. C., Mika, S., Ding, Y. J., Han, T. D., Wu, Q. B., and Yu, Z. B., and Qin D. H., 2016: Diurnal dynamics of minor and trace elements in stream water draining Dongkemadi Glacier on the Tibetan Plateau and its environmental implications. *Journal of Hydrology*, 541: 1104–1118, doi: http://dx.doi.org/10.1016/j.jhydrol.2016.08.021.

Li, Z., Xing, Q., Liu, S. Y., Zhou, J. M., and Huang, L., 2012: Monitoring thickness and volume changes of the Dongkemadi Ice Field on the Qinghai-Tibetan Plateau (1969–2000) using Shuttle Radar Topography Mission and map data. International *Journal of Digital Earth*, 5(6): 516–532, doi: http://dx.doi.org/10.1080/17538947.2011.594099.

Liu, Q., Guo, W. Q., Nie, Y., Liu, S. Y., and Xu, J. L., 2016: Recent glacier and glacial lake changes and their interactions in the Bugyai Kangri, southeast Tibet. *Annals of Glaciology*, 57(71): 61–69, doi: http://dx.doi.org/10.3189/2016AoG71A415.

Liu, S. Y., Yao, X. J., Guo, W. Q., Xu, J. L., Shangguan, D. H., Wei, J. F., Bao, W. J., and Wu, L. Z., 2015: The contemporary glaciers in China based on the Second Chinese Glacier Inventory. *Acta Geographica Sinica*, 70(1): 3–16, doi: http://dx.doi.org/10.11821/dlxb201501001 (in Chinese).

Matsuo, K., and Heki, K., 2010: Time-variable ice loss in Asian high mountains from satellite gravimetry. *International Journal of Educational Development*, 290(1-2): 30–36, doi: http://dx.doi.org/10.1016/j.epsl.2009.11.053.

Neckel, N., Kropáček, J., Bolch, T., and Hochschild, V., 2014: Glacier mass changes on the Tibetan Plateau 2003–2009 derived from ICESat laser altimetry measurements. *Environmental Research Letters*, 9(1): 014009, doi: http://dx.doi.org/10.1088/1748-9326/9/1/014009.

Nuth, C., and Kääb, A., 2011: Co-registration and bias corrections of satellite elevation data sets for quantifying glacier thickness change. *The Cryosphere*, 5(1): 271–290, doi: http://dx.doi.org/10.5194/tc-5-271-2011.

Oerlemans, J., 2005: Extracting a climate signal from 169 glacier records. *Science*, 308(5722): 675–677, doi: http://dx.doi.org/ 10.1126/science.1107046.

Pieczonka, T., and Bolch, T., 2015: Region-wide glacier mass budgets and area changes for the Central Tien Shan between ~1975 and 1999 using Hexagon KH-9 imagery. *Global & Planetary Change*, 128: 1-13, doi: http://dx.doi.org/10.1016/j.gloplacha.2014.11.014.

Pieczonka, T., Bolch, T., Wei, J. F., and Liu, S. Y., 2013: Heterogeneous mass loss of glaciers in the Aksu-Tarim Catchment (Central Tien Shan) revealed by 1976 KH-9 Hexagon and 2009 SPOT-5 stereo imagery. *Remote Sensing of Environment*, 130(4): 233–244, doi: http://dx.doi.org/10.1016/j.rse.2012.11.020.

Pu, J. C., Yao, T. D., Yang, M. X., Tian, L. D., Wang, N. L., Ageta, Y., and Fujita, K., 2008: Rapid decrease of mass balance observed in the Xiao (Lesser) Dongkemadi Glacier, in the central Tibetan Plateau. *Hydrological Processes*, 22(16): 2953–2958, doi: http://dx.doi.org/10.1002/hyp.6865.

Rabus, B., Eineder, M., Roth, A., and Bamler, R., 2003: The shuttle radar topography mission—A new class of digital elevation models acquired by spaceborne radar. *ISPRS Journal of Photogrammetry & Remote Sensing*, 57(4): 241–262, doi: http://dx.doi.org/10.1016/S0924-2716(02)00124-7.

Rignot, E., Echelmeyer, K., and Krabill, W., 2001: Penetration depth of interferometric synthetic-aperture radar signals in snow and ice. *Geophysical Research Letters*, 28(18): 3501–3504, doi: http://dx.doi.org/10.1029/2000GL012484.

Sakai, A., Nishimura, K., Kadota, T., and Takeuchi, N., 2009: Onset of calving at supraglacial lakes on debris-covered glaciers of the Nepal Himalaya. *Journal of Glaciology*, 55(193): 909–917(909), doi: http://dx.doi.org/10.3189/002214309790152555.

Shangguan, D. H, Liu, S. Y., Ding, Y. J., Zhang, Y., Du, E. J., and Wu, Z., 2008: Thinning and retreat of Xiao Dongkemadi glacier, Tibetan Plateau, since 1993. *Journal of Glaciology*, 54(188): 949–951, doi: http://dx.doi.org/10.3189/002214308787780003.

Shangguan, D. H., Bolch, T., Ding, Y. J., Kröhnert, M., Pieczonka, T., Wetzel, H. U., and Liu, S. Y., 2015: Mass changes of Southern and Northern Inylchek Glacier, Central Tian Shan, Kyrgyzstan, during ~1975 and 2007 derived from remote sensing data. *The Cryosphere,* 9(2): 703–717, doi: http://dx.doi.org /10.5194/tc-9-703-2015.

Shi, P. H., Duan, K. Q., Liu, H. C., Yang, J. H., Zhang, X., and Sun, J. Y., 2016: Response of Xiao Dongkemadi Glacier in the central Tibetan Plateau to the current climate change and future scenarios by 2050. *Journal of Mountain Science*, 13(1): 13–28, doi: http://dx.doi.org/10.1007/s11629-015-3609-4.

State Bureau of Surveying and Mapping, 2007: Technical rules for producing digital products of 1:100 000 1:50 000 fundamental geographic information, Part 1: Digital line graphs (DLG), CH/T 1015.1-2007. General Administration of Quality Supervision, Inspection and Quarantine of the People's Republic of China and Standardization Administration of the People's Republic of China. Beijing, China. (In Chinese).

Tian, L., Masson-Delmotte, V., Stievenard, M., Yao, T., and Jouzel, J., 2001: Tibetan Plateau summer monsoon northward extent revealed by measurements of water stable isotopes. *Journal of Geophysical Research–Atmospheres*, 106(D22): 28081–28088, doi: http://dx.doi.org/10.1029/2001JD900186.

Tshering, P., and Fujita., K., 2016: First in situ record of decadal glacier mass balance (2003–2014) from the Bhutan

Himalaya. *Annals of Glaciology*, 57(71): 289, doi: http://dx.doi.org/10.3189/2016AoG71A036.

Wang, C. Q., Yang, T. B., Qin, J. I., and Yi, H. E., 2016: Remote sensing monitoring of glacier changes in the middle region of Tanggula Mountain. *Arid Land Geography*, 39(3): 504–5012, doi: http://dx.doi.org/10.13826/j.cnki.cn65-1103/x.2016.03.006 (in Chinese).

Wang, N. L., He, J. Q., Pu, J. C., Jiang, X., and Jing, Z. F., 2010: Variations in equilibrium line altitude of the Qiyi Glacier, Qilian Mountains, over the past 50 years. *Science Bulletin*, 55(33): 3810–3817, doi: http://dx.doi.org/10.1007/s11434-010-4167-3.

Wang, P.Y., Li, Z. Q, Wang, W. B., Li, H. L., Zhou, P., and Jin, S., 2013: Changes of six selected glaciers in the Tomor region, Tian Shan, Central Asia, over the past ~50 years, using high-resolution remote sensing images and field surveying. *Quaternary International*, 311: 123–131, doi: http://dx.doi.org/10.1016/j.quaint.2013.04.031.

Wei, J. F., Liu, S.Y., Xu, J. L., Guo, W. Q., Bao, W. J., Shangguan, D. H., and Jiang, Z. L., 2015: Mass loss from glaciers in the Chinese Altai Mountains between 1959 and 2008 revealed based on historical maps, SRTM, and ASTER images. *Journal of Mountain Science*, 12(2): 330–343, doi: http://dx.doi.org/10.1007/s11629-014-3175-1.

Wiltshire, A. J., 2014: Climate change implications for the glaciers of the Hindu-Kush, Karakoram and Himalayan region. The Cryosphere, 8(3): 941–958, doi: http://dx.doi.org/ 10.5194/tc-8-941-2014.

Wu, X. J., Wang, N. L., Lu, A. X., Pu, J. C., Guo, Z. M., and Zhang, H. W., 2015: Variations in albedo on Dongkemadi Glacier in Tanggula Range on the Tibetan Plateau during 2002–2012 and its linkage with mass balance. *Arctic, Antarctic, and Alpine Research*, 47(2): 281–292, doi: http://dx.doi.org/10.1657/AAAR00C-13-307.

Yao, T. D., Pu, J. C., Lu, A. X , Wang, Y. Q., and Yu, W. S., 2007: Recent glacial retreat and its impact on hydrological processes on the Tibetan Plateau, China, and surrounding regions. *Arctic, Antarctic, and Alpine Research*, 39(4): 642–650, doi: http://dx.doi.org/10.1657/1523-0430(07-510)[YAO]2.0.CO;2.

Yao, T. D., Li, Z. G., Yang, W., Guo, X. J., Zhu, L. P., Kang, S. C., Wu, Y. H., and Yu, W. S., 2010a: Glacial distribution and mass balance in the Yarlung Zangbo River and its influence on lakes. *Science Bulletin*, 55(20): 2072–2078, doi: http://dx.doi.org/10.1007/s11434-010-3213-5.

Yao, T., Thompson, L., Yang, W., Yu, W., Gao, Y., Guo, X., Yang, X., Duan, K., Zhao, H., and Xu, B., 2012: Different glacier status with atmospheric circulations in Tibetan Plateau and surroundings. *Nature Climate Change*, 2(9): 663–667, doi: http://dx.doi.org/10.1038/nclimate1580.

Yao, T. D., Zhang, Y. S., Pu, J. C., Tian, L. D., Ageta, Y., and Ohata, T., 2010b: Twenty-year observations of glacier, hydrology and meteorology at the Tanggula Pass of the Tibetan Plateau: Significance and achievements. *Journal of Glaciology & Geocryology*, 32(6): 1152–1161 (in Chinese).

Ye, Q. H., Kang, S. C., Chen, F., and Wang, J. H., 2006: Monitoring glacier variations on Geladandong mountain, central Tibetan Plateau, from 1969 to 2002 using remote-sensing and GIS technologies. *Journal of Glaciology*, 52(179): 537–545, doi: http://dx.doi.org/10.3189/172756506781828359.

Yi, S., and Sun, W., 2014: Evaluation of glacier changes in high-mountain Asia based on 10 year GRACE RL05 models. *Journal of Geophysical Research–Solid Earth*, 119(3): 2504–2517, doi: http://dx.doi.org/10.1002/2013JB010860.

Yu, W. S., Yao, T. D., Kang, S. C., Pu, J. C., Yang, W., Gao, T. G., Zhao, H. B., Zhou, H., Li, S. H., and Wang, W. C., 2013: Different region climate regimes and topography affect the changes in area and mass balance of glaciers on the north and south slopes of the same glacierized massif (the West Nyainqentanglha Range, Tibetan Plateau). *Journal of Hydrology*, 495(2): 64–73, doi: http://dx.doi.org/10.1016/j.jhydrol.2013.04.034.

Zemp, M., Hoelzle, M., and Haeberli, W., 2009: Six decades of glacier mass-balance observations: a review of the worldwide monitoring network. *Annals of Glaciology,* 50(50): 101–111, doi: http://dx.doi.org/10.3189/172756409787769591.

Zemp, M., Nussbaumer, S. U., Naegeli, K., Gärtnerroer, I., Paul, F., Hoelzle, M., and Haeberli, W., 2013: Glacier Mass Balance Bulletin No. 12 (2010–2011).

Zemp, M., Frey, H., Gärtnerroer, I., Nussbaumer, S. U., Hoelzle, M., Paul, F., Haeberli, W., Denzinger, F., Ahlstrøm, A. P., and Anderson, B., 2015: Historically unprecedented global glacier decline in the early 21st century. *Journal of Glaciology*, 61(228): 745–762, doi: http://dx.doi.org/10.3189/2015JoG15J017.

MS submitted 13 October 2016
MS accepted 7 July 2017

APPENDIX

TABLE A1

Characteristics of the glaciers investigated in this study, based on the Second Glacier Inventory Dataset of China.

Region	GLIMS_ID	Long (degree)	Lat (degree)	Area (km^2)	Min_Elev (m)	Med_Elev (m)	Slope (degree)	Aspect (degree)
Dongkemadi	G092105E33116N	92.105	33.116	5.8	5288.9	5574.9	13.3	95.8
	G092106E33096N	92.106	33.096	2.8	5346.9	5583.9	13.9	95.2
	G092110E33135N	92.110	33.135	1.2	5416.0	5647.0	19.6	113.8
	G092014E33147N	92.014	33.147	0.5	5383.7	5569.7	23.7	35.9
	G092017E33093N	92.017	33.093	0.1	5547.0	5655.0	23.0	331.5
	G092020E33141N	92.020	33.141	1.3	5302.4	5567.4	16.6	32.4
	G092021E33088N	92.021	33.088	0.4	5516.9	5707.9	18.3	252.4
	G092022E33094N	92.022	33.094	0.3	5382.5	5653.5	21.4	343.3
	G092028E33083N	92.028	33.083	1.0	5452.9	5714.9	19.2	236.9
	G092032E33095N	92.032	33.095	1.7	5301.8	5633.8	22.2	352.8
	G092037E33139N	92.037	33.139	2.9	5269.8	5553.8	15.8	349.5
	G092040E33099N	92.040	33.099	0.1	5731.3	5867.3	26.8	266.8
	G092054E33149N	92.054	33.149	1.4	5308.9	5596.9	16.3	8.8
	G092063E33116N	92.063	33.116	19.4	5241.0	5637.0	10.4	273.8
	G092063E33082N	92.063	33.082	16.0	5280.9	5666.9	12.0	183.5
	G092071E33148N	92.071	33.148	4.4	5263.4	5610.4	12.3	2.7
	G092093E33145N[A]	92.093	33.145	6.5	5277.6	5599.6	10.5	0.4
	G092096E33078N	92.096	33.078	5.6	5292.8	5618.8	10.4	167.8
	G092112E33153N[B]	92.112	33.153	2.4	5374.8	5571.8	11.5	30.5
Bugyai Kangri	G094626E31817N	94.626	31.817	2.7	4908.1	5544.1	25.1	208.2
	G094626E31837N	94.626	31.837	4.3	4874.9	5623.9	21.3	293.6
	G094631E31856N	94.631	31.856	1.9	4939.4	5519.4	26.4	310.6
	G094638E31869N	94.638	31.869	1.6	5073.2	5383.2	20.9	332.4
	G094667E31807N	94.667	31.807	35.5	4190.4	5702.4	17.0	213.0
	G094692E31769N	94.692	31.769	1.6	5105.8	5381.8	19.7	200.6
	G094702E31775N	94.702	31.775	0.8	5023.1	5554.1	29.4	171.2
	G094728E31782N	94.728	31.782	22.3	4328.3	5796.3	18.9	176.2
	G094767E31791N	94.767	31.791	1.5	4875.1	5193.1	22.3	117.8
	G094809E31808N	94.809	31.808	4.4	4790.7	5400.7	24.1	48.0
	G094659E31864N	94.659	31.864	2.3	4907.3	5398.3	29.4	23.2
	G094684E31847N	94.684	31.847	15.4	4678.4	5558.4	18.3	27.2
	G094720E31839N	94.720	31.839	9.4	4785.4	5590.4	17.6	26.6
	G094745E31824N	94.745	31.824	13.6	4618.2	5597.2	18.0	36.9
	G094775E31816N	94.775	31.816	10.1	4820.2	5348.2	15.0	30.6
	G094796E31823N	94.796	31.823	1.1	5129.6	5377.6	18.9	349.6

TABLE A1

(Continued)

Region	GLIMS_ID	Long (degree)	Lat (degree)	Area (km^2)	Min_Elev (m)	Med_Elev (m)	Slope (degree)	Aspect (degree)
West-Geladandong	G090854E33544N	90.854	33.544	2.7	5360.8	5661.8	18.9	345.0
	G090878E33547N	90.878	33.547	5.7	5323.5	5741.5	16.4	7.5
	G090890E33413N	90.890	33.413	16.1	5406.1	5704.1	7.4	105.9
	G090891E33555N	90.891	33.555	1.0	5500.8	5758.8	20.3	303.7
	G090896E33572N	90.896	33.572	3.0	5391.0	5698.0	13.6	348.4
	G090901E33443N[D]	90.901	33.443	11.4	5403.2	5838.2	12.7	138.6
	G090903E33508N	90.903	33.508	4.3	5448.9	5825.9	16.0	86.1
	G090911E33545N	90.911	33.545	12.8	5331.5	5693.5	12.1	47.1
	G090911E33519N	90.911	33.519	4.8	5435.2	5760.2	12.6	121.6
	G090913E33483N	90.913	33.483	1.5	5651.9	5910.9	13.8	127.4
	G090916E33469N	90.916	33.469	8.6	5409.3	5764.3	15.8	83.2
	G090917E33492N	90.917	33.492	4.8	5391.2	5759.2	16.5	63.3
	G090921E33452N	90.921	33.452	2.3	5529.3	5836.3	14.7	129.8
	G090934E33529N	90.934	33.529	4.4	5409.3	5744.3	15.0	77.5
	G090807E33440N	90.807	33.440	1.3	5596.2	5692.2	11.5	96.5
	G090819E33418N	90.819	33.418	1.0	5495.8	5759.8	11.4	267.9
	G090830E33408N	90.830	33.408	2.8	5458.2	5810.2	9.7	262.4
	G090838E33394N	90.838	33.394	3.2	5415.9	5693.9	8.0	249.8
	G090840E33469N	90.840	33.469	2.4	5550.7	5856.7	17.1	257.9
	G090842E33532N	90.842	33.532	1.3	5526.5	5724.5	17.2	300.8
	G090847E33480N[C]	90.847	33.480	9.0	5379.1	5851.1	14.3	314.7
	G090847E33437N	90.847	33.437	29.8	5379.1	5779.1	10.8	305.7
	G090852E33393N	90.852	33.393	0.5	5566.3	5843.3	12.6	208.6
	G090858E33379N	90.858	33.379	6.3	5404.5	5713.5	7.8	274.1
	G090866E33502N	90.866	33.502	27.8	5318.1	5782.1	13.4	300.8
	G090884E33381N	90.884	33.381	7.4	5362.7	5652.7	6.3	134.2

Note: [A, B, C,] and [D] represent the Glaciers A, B, C and D, respectively; Long and Lat represent the longitude and latitude, respectively; Min_Elev and Med_Elev represent the minimum and median elevations, respectively.

TABLE A2

Mass budgets of glaciers A and B during the periods 1969–1999, 1999–2015, and 1969–2015.

		Mass balance (m w.e. a^{-1})		
Name	GLIMS_ID	1969–1999	1999–2015	1969–2015
A	G092093E33145N	0.03±0.07	–0.33±0.03	–0.25±0.03
B	G092112E33153N	0.04±0.07	–0.33±0.03	–0.24±0.03

Note: The detailed information of glaciers A and B are shown in the Table A1.